33RD CONGRESS
OF THE INTERNATIONAL COUNCIL
OF THE AERONAUTICAL SCIENCES
STOCKHOLM, SWEDEN, 4-9 SEPTEMBER, 2022

ICAS 2022 SWEDEN

INFLUENCE OF TIP DIHEDRAL ON ROTOR AERODYNAMIC PERFORMANCE AND TIP VOTEX

Minghui Kang[1, 2], Xu Zhao[1, 2], Rui Yao[1, 2], Hongyan Li[1, 2]

[1] *National Key Laboratory of Science and Technology on Aerodynamic Design and Research, Northwestern Polytechnical University, Xi'an, Shaanxi, 710072, China*

[2] *School of Aeronautics, Northwestern Polytechnical University, Xi'an, Shaanxi, 710072, China*

Abstract

The geometry of the rotor is the main factor affecting the aerodynamic characteristics of the rotor. As one of the main aerodynamic parameters of the blade, the tip is the most sensitive area of the blade. Studies have shown that the dihedral angle of the propeller tip is beneficial to reduce propeller-vortex interference. The formed rotating twin vortices collide and merge before reaching the next blade, which weakens the strength of the tip vortex and reduces the propeller-vortex interference. At the same time, the tip vortex has an inductive effect on the inflow of the rotor, so it will have a significant impact on the lift distribution of the blade. In this paper, aiming at the research on the aerodynamic characteristics and flow field of the helicopter rotor by the shape of the blade tip, the research on the aerodynamic shape performance of the double-swept lower reverse blade tip with sharpening will be carried out. The CFD simulation and experiment methods were used to evaluate the optimal tip shape of the rotor under the selected operating conditions, and to study the influence of the dihedral angle on the tip twin vortices.

Keywords: rotor, tip dihedral, vortex, PIV

1. Introduction

Scholars have long begun to pay attention to the influence of the paddle tip shape on the aerodynamic performance and noise of the rotor.

Muller[1]observed the opposite twin vortex structure through the smoke flow in the wind tunnel experiment, and the twin vortices collided and merged before the subsequent blades met, thereby weakening the strength of the tip vortex. Brocklehurst and Barakos [2]reviewed the research on the shape of helicopter propeller tips. The generation of opposite twin vortices is a passively controlled vortex method, and the downward inversion of the propeller tip is one of the most effective methods. The British Experimental Rotor Programme (BERP) tip adopts a double-sweep and downward-reverse tip design, which makes the rotor pulling force 30%~40% higher than that of conventional blades[3], and optimizes the aerodynamic characteristics of the rotor. The ERATO blade reduces BVI noise by optimizing the spanwise distribution of chord length and adopting a double-sweep, sharp and dihedral blade tip configuration which can be seen that the three-dimensional configuration of the lower tip of the tip effectively weakens the strength of the tip vortex and improves the aerodynamic characteristics of the rotor[4].

At present, the research methods of rotor aerodynamics are mainly wind tunnel test, flight test and CFD simulation. In this paper, referring to the advanced rotor geometry, the CFD numerical analysis of the designed rotor hovering flow field is carried out, and the appropriate working conditions are selected. Subsequently, a physical model will be made through 3D printing technology for wind tunnel testing.

2. Numerical Analysis Methods

2.1 Control Equations

This paper mainly adopts the Reynolds-averaged Navier-Stokes equation as the basic governing equation. In the inertial Cartesian coordinate system, the conserved integral form of the three-dimensional compressible unsteady N-S equations ignoring the body force and heat source is:

$$\frac{\partial}{\partial t}\iiint_{\Omega}\vec{Q}dV+\iint_{\partial\Omega}\vec{F_c}\cdot\vec{n}\,dS-\iint_{\partial\Omega}\vec{F_v}\cdot\vec{n}dS=0 \tag{1}$$

In the formula(1), Ω is any control volume in the flow field space; $\partial\Omega$ is the boundary of the control volume; dS is the surface element on the boundary; $\vec{Q}$ represents the conserved variable, $\vec{F_c}$ represents the inviscid flux, and $\vec{F_v}$ represents the viscous flux.

The above equations are solved discretely by the finite volume method, the gradient term is discretized by the least squares method, the turbulent kinetic energy is discretized by the first-order upwind style, and the turbulent dissipation rate is discretized by the first-order upwind style. The viscous term is discretized using the second-order central difference format, and the non-sticky term is discretized using the Roe-FDS format.

2.2 Turbulence Model

When the traditional RANS method is used to numerically simulate the rotor tip vortex, the excessive numerical viscosity causes the rotor tip vortex to be seriously dissipated in the calculation process. Aiming at the inadequacy of the RANS method to simulate the complex turbulent flow, the IDDES method is used to numerically simulate the rotor turbulent separation flow. The RANS method is used in the flow area characterized by dissipation, and the LES method is used in the area characterized by large eddy transport. Compared with the unsteady RANS method, the IDDES method captures the small-scale vortex structure in the flow field[5].

2.3 Sliding Mesh

In this paper, the sliding mesh is used to realize the numerical simulation of the RANS/LES hybrid method. Compared with the point-joined mesh, the node distribution can be discontinuous at the overlapped surface, which can greatly reduce the amount of computation, thereby saving computing resources, and focusing the computing grid on the key areas of encryption. When the slip grid is applied to the flow field calculation, the complexity of the calculation is simplified, and it has high reliability and accuracy.

The computational domain takes the cylindrical flow field and is divided into rotating domain I and static domain II, as shown in Figure 1.

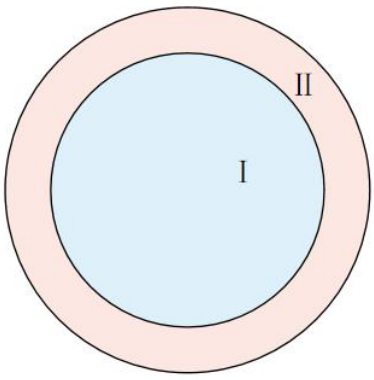

Figure 1 – Computational domain.

3. Example Verification

3.1 Caradonna-Tung Rotor Model

The Caradonna-Tung[6] rotor model is a standard example for rotor calculation at present. In order to verify the applicability of the rotor flow field CFD analysis method used in this paper to the unsteady flow field calculation, the flow of the Caradonna-Tung rotor in the hovering state is calculated and analyzed. field. The Caradonna-Tung rotor model consists of two non-twisted, rectangular blades (Figure 2).

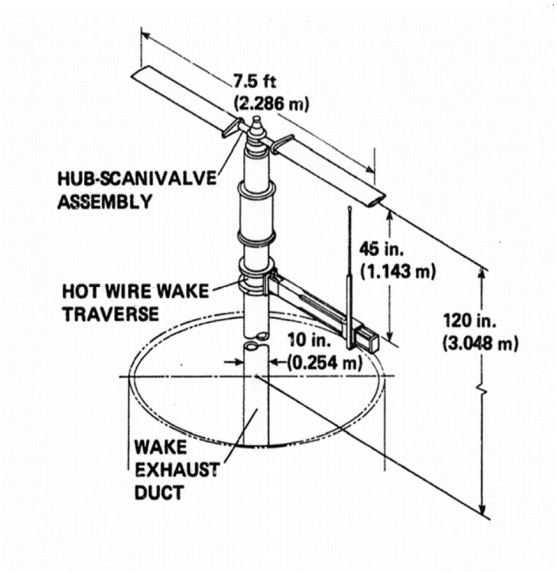

Figure 2 – Schematic diagram of the Caradonna-Tung experimental model[6] .

Ignoring the influence of the hub and connecting rod, the C-T rotor with the tip Mach number Mtip=0.612 was selected for numerical simulation analysis. The experimental parameters are shown in Table 1.

Table 1 – Caradonna-Tung rotor parameters.

Rotor parameters	Value	Rotor parameters	Value
Radius R/m	1.143	Aerofoil	NACA0012
Chord c/m	0.1905	Speed Ω/(rpm)	1750
Blade root cutting	0.1R	Collective pitchθ/(°)	8
Number of blades	2	Rotor solidity σ	0.1061

3.2 Computational Grid

The rotating domain is a small cylinder that surrounds the blade and is coaxial with the paddle disc. The distance in the radial direction is 2R, the distance in the upstream direction is 1R, and the distance in the downstream direction is 2R; the static domain II is a large cylinder surrounding the small cylinder and coaxial with it. , the distance in the radial direction is 15R, the distance in the upstream direction is 15R, and the distance in the downstream direction is 20R. The meshes are constructed separately for the rotating domain and the stationary domain, and the two are overlapped by the interface. The mesh of the first layer is 10-5c, and the overall mesh number is 473W.

Figure 3 shows the details of the structural mesh at the blade tip. It can be seen from the figure

that the boundary layer mesh transition on the blade is good.

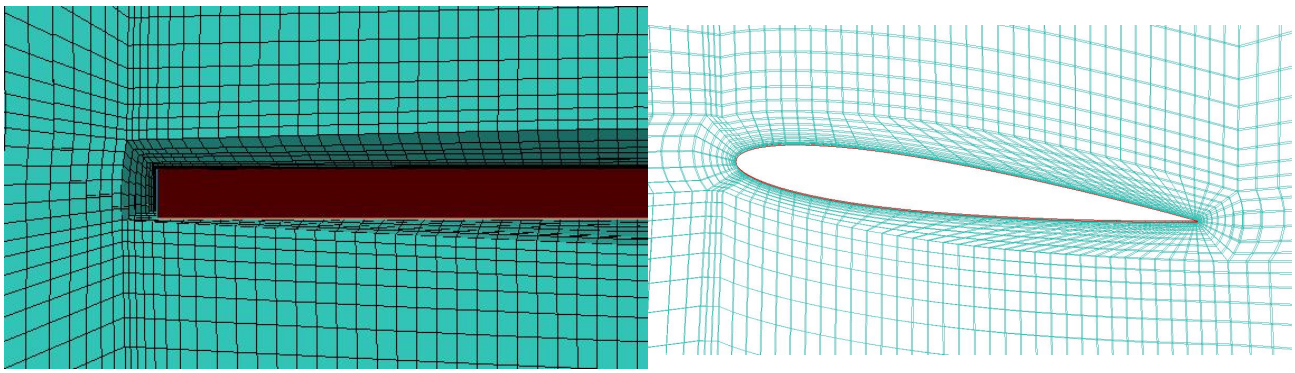

Figure 3 – Blade tip mesh.

3.3 Numerical Simulation Results and Analysis

The formula for calculating the pressure coefficient of the rotor blade surface is:

$$C_p = \frac{p - p_\infty}{0.5\rho_\infty\left(r\Omega + \mu\Omega R\sin\varphi\right)} \tag{2}$$

Figure 4 shows the comparison between the calculated value and the experimental value of the average pressure coefficient distribution at different sections of the blade and at each moment. Among them, the ordinate CP is the pressure coefficient; the abscissa x/c is the ratio of the dimension-normalized local coordinate to the local chord length; r/R is the coordinate of the section along the radius.

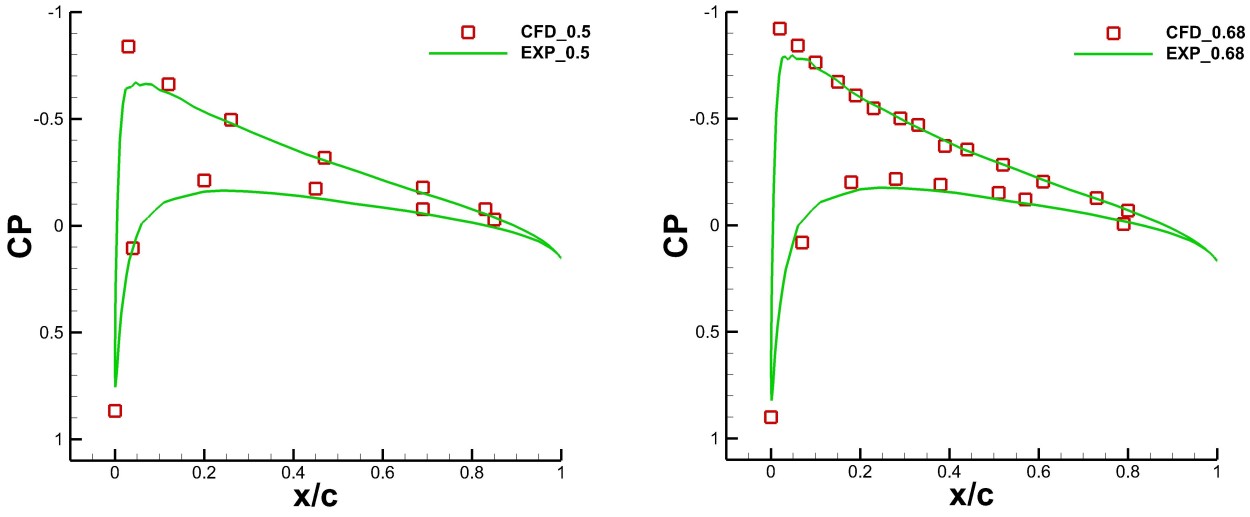

(a) r/R=0.5

(b) r/R=0.68

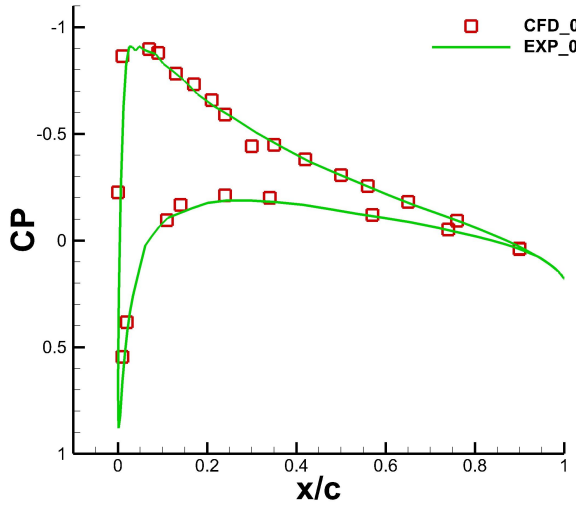

(b) r/R=0.8

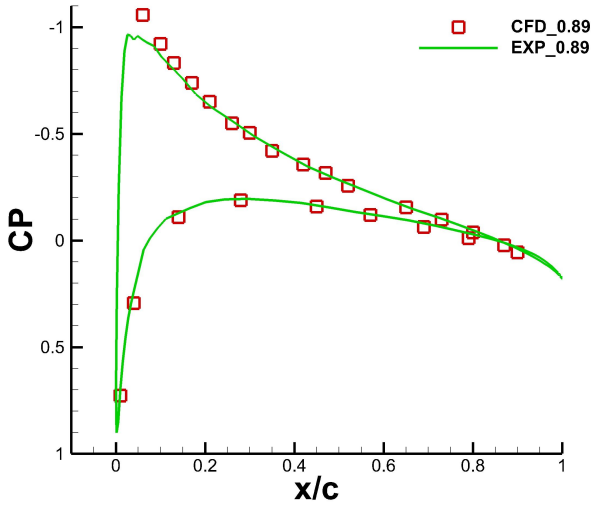

(d) r/R=0.89

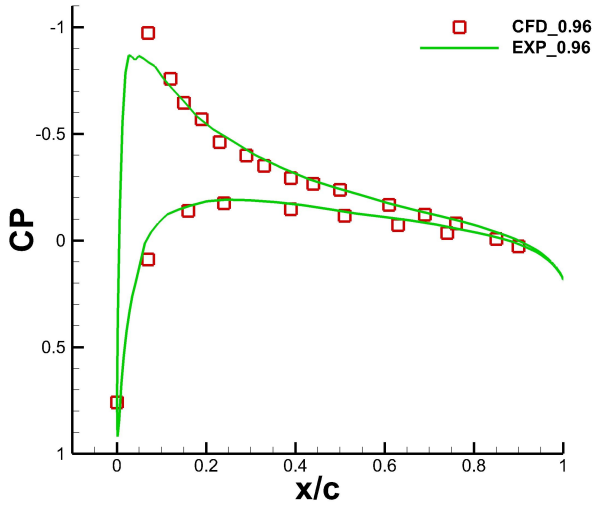

(e) r/R=0.96

Figure 3 – Pressure coefficient distributions of Caradonna-Tung.

From the pressure coefficient curves of the five sections, it can be seen that the numerical simulation results in this paper are basically consistent with the curve trend of the experimental values of the C-T rotor, and have a good consistency.

Figure 5 shows the isovorticity plots stained with axial velocity, and Figure 6 shows the axial slice vorticity distribution of the rotor under the Q criterion.

At the same time, the vortex core position of Caradonna-Tung was extracted and compared with the experimental data. It can be seen from Figure 7 that the movement trend of the vortex core position calculated by CFD is consistent with the experimental data, which proves that the above numerical simulation method can accurately describe The morphological characteristics and motion law of the vortex.

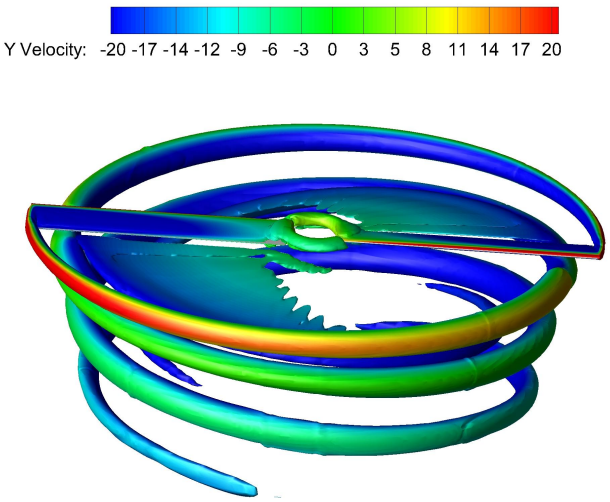

Figure 5 – Isovorticity plots.

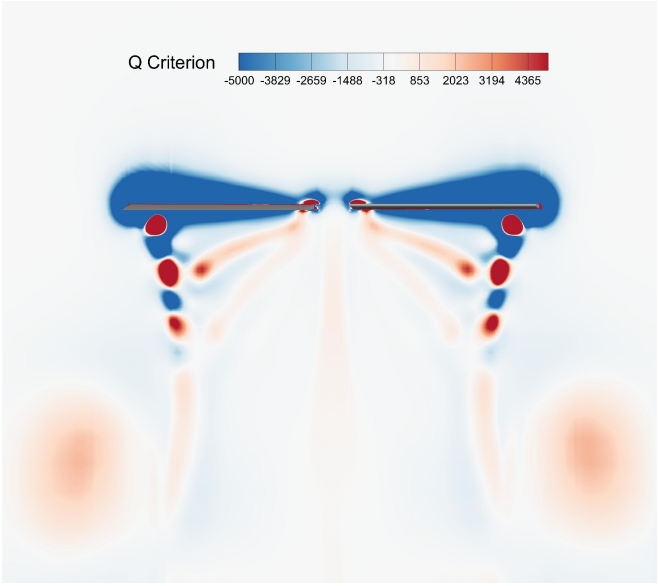

Figure 6 –Axial slice vorticity.

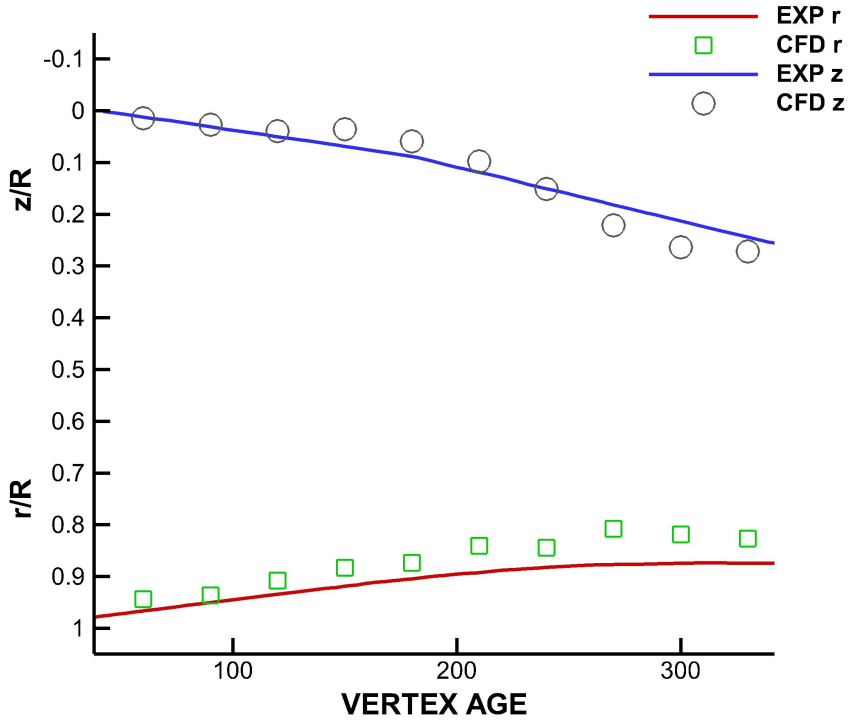

Figure 7 – Vortex core position comparison.

It is proved that the calculation accuracy of the adopted method meets the engineering requirements and can be used for the subsequent analysis and optimization of rotor aerodynamic characteristics.

4. Designed Rotor Blade

4.1 Blade Shape Design

The blade design refers to the shape of the ERATO blade, and adopts the double-swept blade tip plane shape that delays shock generation and reduces rotor noise as the basic configuration. The airfoil is selected from ONERA's OA213 airfoil (Figure 8).

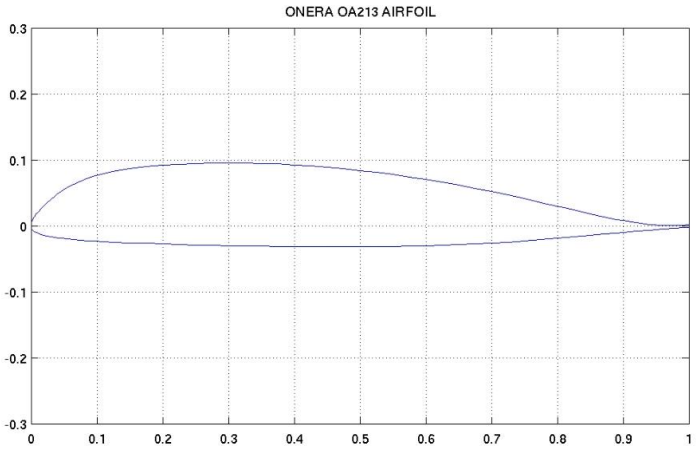

Figure 8 – ONERA OA213 airfoil.

Considering that the wind tunnel test of the designed rotor will be carried out in the future, the size and shape of the rotor are restricted by the wind tunnel conditions. On the basis of satisfying the experimental conditions and processing conditions, the aspect ratio of the designed rotor blade is set to 9, and the root chord length c= 0.1m. The schematic diagram of the blade model is shown in the Figure 9.

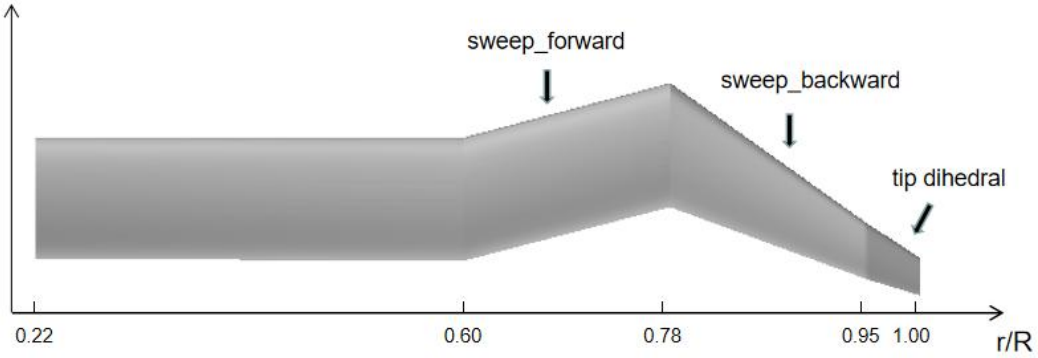

Figure 9 – Designed blade model.

Referring to the optimized design results of Dong Qi et al. [7], the design range of the propeller tip is 0.6R~1.0R of the rotor radius. The range of the forward swept part is 0.6R~0.781R, and the range of the back swept part is 0.9R~1.0R, and the forward swept amount is selected to be 0.44 times of the local chord length.

The cutting of the blade tip will reduce the chord length and thickness of the airfoil at the blade tip, and the effective bearing area of the blade tip will decrease, which can increase the induced velocity in the inner area of the blade disc and weaken the blade tip interference. The research shows that the induced drag factor decreases with the increase of the sharpening ratio in the range of small angle of attack, while in the range of large angle of attack, the induced resistance factor increases with the increase of the sharpening ratio. After comprehensive consideration The tip ratio of the rotor blade is selected as λ=0.3, and the starting position of the tip is the same as the

starting position of the sweep. The blades have -9° linear negative twist.

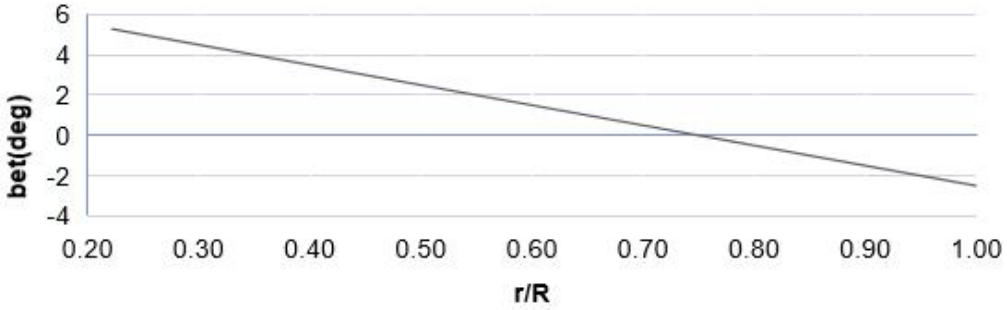

Figure 10 – Twist angle of designed blade.

Studies have shown that the downturn of the rotor blade tip can significantly reduce the impact range of the shock wave and reduce the shock wave intensity (Sun Mengxin). When the pulling force is small, the hovering efficiency is improved when the lower reverse starting position is close to the tip of the propeller, and the hovering efficiency is reduced when it is close to the root of the propeller. And the hovering efficiency increases first and then decreases with the increase of the downward anti-angle. Therefore, the lower inversion position of the designed rotor is at 0.95R, and the lower inversion angle is changed within a certain range to find the most suitable model for experiments.

4.2 Numerical Simulation

4.2.1 Working Condition Selection

In order to save computing resources and improve computing efficiency, the optimal working conditions for designing the rotor are firstly screened out through steady calculation. Constantly calculate the rotors at three different lower angles such as 5°, 10°, 15° and four different installation angles such as 7°, 9°, 11°, 13°, and compare the rotors with and without torsion difference in aerodynamic performance. Set the rotor speed to 1000rpm, and the tip Mach number M_{tip}=0.277. The hover efficiency is used as the main reference value for comparison, and the results are shown in the Figure 11. On the whole, the rotor with twist is more efficient than the rotor without twist. The optimal installation angle of the rotor is 11°, and the hovering efficiency is the highest when the dihedral angle is 15°.

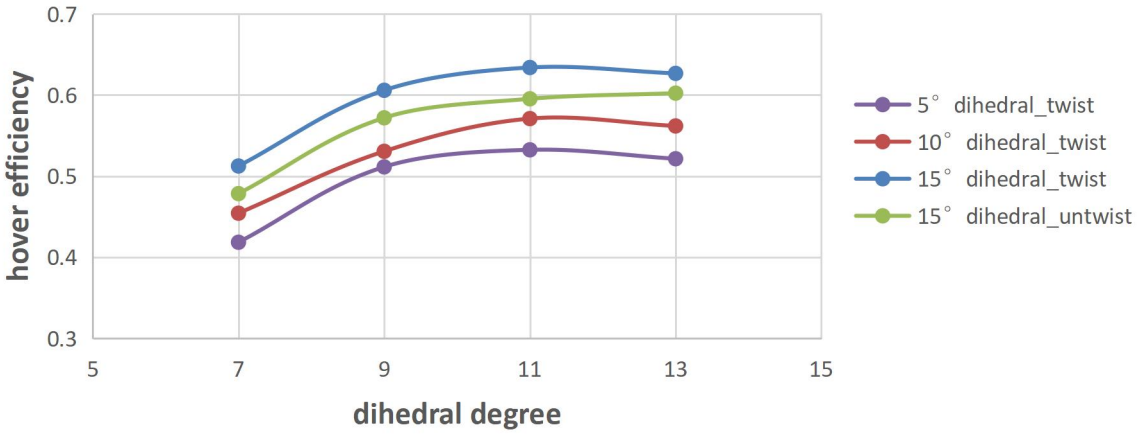

Figure 11 – Comparison of hovering efficiency under different working conditions.

4.2.2 Unsteady numerical simulation

This subsection will perform high-precision numerical simulations for a 15° dihedral rotor with twist model.

The CFD simulation of the flow around the blade applies the high-precision simulation method to capture rotor tip vortex, based on the sliding mesh and adaptive grid methods,Special treatment, the spatial discretization adopts the combination of the second-order upwind monotonic conservation scheme and the flux difference splitting method. The rotor CFD simulation under the hovering condition adopts the sliding grid technology, the time discretization adopts the second-order accuracy or higher, the time step during hovering is taken as the value corresponding to the 1°rotation of the rotor, the flow model adopts IDDES, and the collective pitch and rotational speed are known. Rotor pull, power, hover efficiency, wake and tip vortex in preparation for hover performance measurements will be predicted and compared with flow field experiments. It is proposed to use multi-grid technology to accelerate the convergence. Implicit solution is used in the blade tip area, and local time advancement, control of the number of CFL, and parallel computing will also be adopted.

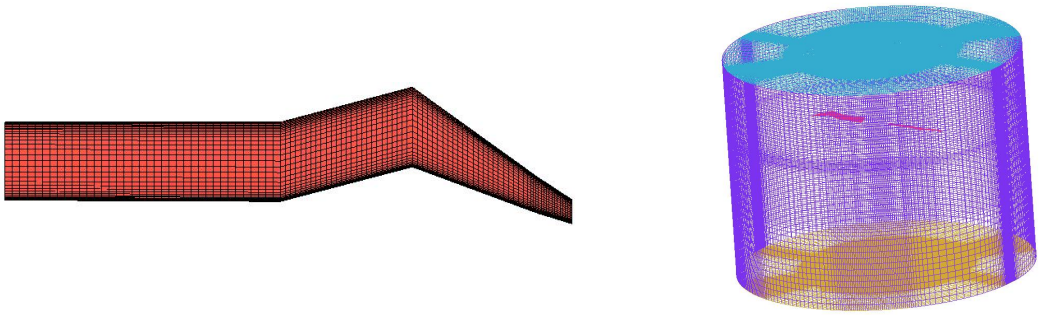

Figure 12 – Blade surface mesh and rotating domain mesh.

The Figure 12 shows the surface mesh of the rotor blade and the mesh of the rotating domain. The mesh is refined at the downstream position of the flow, and the overall mesh amount of the calculated flow field is 586W.

After calculation, the obtained surface pressure and tip pressure distribution of the designed blade are shown in Figure 13.

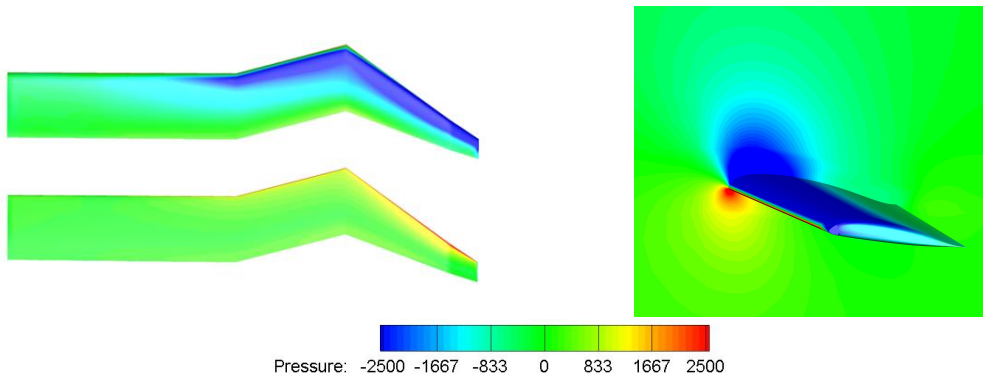

Figure 13 – Pressure contours at blade tip section.

4.3 Experiment Design of Rotor

4.3.1 Experiment equipment and method

The rotor test will be carried out on the 2m rotor test rig of the National Key Laboratory of Rotorcraft Aeromechanics. The hovering aerodynamic performance test of two model rotors with no lower reverse design rotor and 15° lower reverse design rotor will be carried out. The rotor is installed on the bracket of the test bench, and the rotor is driven by a DC motor. The plane of the

paddle is 2.6m from the ground. The collective pitch angle of the rotor is adjusted within a specified range, and the rotational speed is fixed to measure the rotor pull and torque under different working conditions to test and compare the rotor performance under different working conditions.

Figure 14 – Position of model rotor on rotor test rig during experiment[8].

The pulling force of the model rotor will be measured by a six-component balance, and the torque will be measured by a torque balance. The dimensionless lift coefficient C_T and torque coefficient m_k in the test are defined as formula 3.

$$C_T = T/[\frac{1}{2}\rho\pi R^2(\Omega R)^2]$$
$$m_k = M_k/[\frac{1}{2}\rho\pi R^2(\Omega R)^2 R] \quad (3)$$

Figure 15 shows the schematic diagram of the measurement and processing system in the experiment.

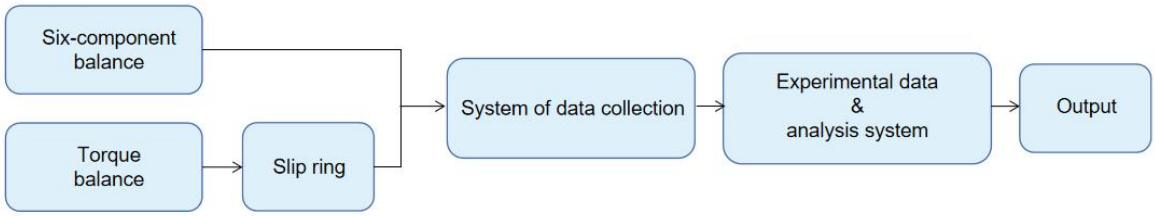

Figure 15 – Schematic flow chart of measuring and processing system.

4.3.2 Calibration of the rotor test rig

Since the model rotor test rig may have ground effects or interference, the error of the test rig needs to be corrected. It is proposed to tilt the rotor platform at a certain angle to study the changes of the model rotor lift coefficient and torque coefficient under the same conditions.

Expected results of this paper includes:

(1) Influence rule of dihedral angle on generation and evolution of propeller tip vortex.

(2) Flow field measurement of the flow around the lower dihedral tip based on PIV technology.

(3) Study on the evolution of vortex core position and intensity.

(4) Study on the mutual interference and merging process of twin vortices.

5. Conclusion

Based on the CFD numerical simulation of the unsteady rotor flow field, this paper uses the slip grid method to verify the Carannda-Tung rotor example. The calculation results are in good agreement with the experimental data. Taking into account the influence of the rotor blade torsion, forward swept, backward swept, sharp cut, dihedral and other shapes, the aerodynamic characteristics of the rotor under different parameters were analyzed, which laid the foundation for the subsequent rotor wind tunnel experiments.

6. Contact Author Email Address

Mailto: xuzhao@nwpu.edu.cn

7. Copyright Statement

References

[1] Muller R.H.G. (1987) The influence of winglets on rotor aerodynamics, 12 European Rotorcraft Forum, Garmisch-Partenkirchen, Germany.

[2] Brocklehurst A. and Barakos G.N. (2013), A review of helicopter rotor blade tip shapes，Progress in Aerospace Sciences 56，35–74.

[3] Harrison R.，Stacey S (2008). BERP IV –the design, development and testing of an advanced rotor blade. Proceedings of American Helicopter Society Annual Forum, 64(2):1334.

[4] A. Le Pape, P. Beaumier,Numerical optimization of helicopter rotor aerodynamic performance in hover,Aerospace Science and Technology,Volume 9, Issue 3,2005,Pages 191-201,ISSN 1270-9638.

[5] FU Weijia, MA Jingzhong, LI Jie. Investigation of Rotor Tip Vortex in Hover Based on IDDES Methods. Journal of Northwestern Polytechnical University, 2019, 37(1): 195-202.

[6] Caradonna F X，Tung C.Experimental and analytical studies of a model helicopter rotor in hover[J].Vertica，1981，5(2)：149-161.

[7] 董琦, et al."旋翼低噪声双掠桨尖优化设计方法研究".2016年度全国气动声学学术会议论文摘要集.Ed.. , 2016, 240-249.

[8] 招启军,徐国华.新型桨尖旋翼悬停气动性能试验及数值研究[J].航空学报,2009,30(03):422-429.ISSN:1000-6893.